Hindawi
Structural Control and Health Monitoring
Volume 2023, Article ID 9748991, 16 pages
https://doi.org/10.1155/2023/9748991

Research Article

Pounding Mitigation Design and Real-Time Hybrid Simulation for a Novel Viscous Damper Applied in Bridges

Yong Ding,[1,2,3] **Yifei Zhang**,[1,2,3] **and Guoshan Xu**[1,2,3]

[1]*School of Civil Engineering, Harbin Institute of Technology, Harbin 150090, China*
[2]*Key Lab of Structures Dynamic Behavior and Control, Ministry of Education, Harbin Institute of Technology, Harbin 150090, China*
[3]*Key Lab of Intelligent Disaster Mitigation, Ministry of Industry and Information Technology, Harbin 150090, China*

Correspondence should be addressed to Guoshan Xu; xuguoshan@hit.edu.cn

Received 25 January 2023; Revised 19 April 2023; Accepted 26 April 2023; Published 8 May 2023

Academic Editor: Fabio Casciati

When the actual displacement of viscous damper exceeds the stroke limit, excessive pounding force may be generated, resulting in damage to the damper. To address this issue, a novel viscous damper with variable stiffness, simple processing, and good economy is proposed. First, the load-displacement relation of the novel viscous damper is established through theoretical analysis and experimental studies. Second, numerical simulations and a series of parametric analyses are conducted to analyze the pounding mitigation effect of the proposed damper. Third, real-time hybrid simulation (RTHS) for considering the pounding effect of the novel viscous damper is presented. Finally, design recommendations for the pounding mitigation design of the novel viscous damper are given. The results show that the novel viscous damper effectively reduces the amplitudes of the pounding force and acceleration by 25% and 24%, respectively. The Fourier power of acceleration decreases in the region from 0.6 Hz to 3.3 Hz. The results of RTHS demonstrate that the real-time hybrid testing system can effectively simulate the pounding effect of the proposed damper. However, the normalized error peak value of velocity between RTHS and the reference result exceeds 10%, indicating that the proposed damper considering the pounding effect imposes new requirements to the real-time hybrid testing method.

1. Introduction

1.1. Background and Motivation. In recent years, there have been frequent instances of pounding and unseating of bridge superstructures during earthquakes. For example, a 7.4 magnitude earthquake occurred in Maduo County, Qinghai, China, on May 22, 2021, resulting in the unseating of 70% of the total spans of the Yematan Bridge, located to the south of the fault [1]. In order to effectively control structural vibration, researchers have proposed a variety of passive energy dissipation devices and design strategies [2–11]. Among them, viscous dampers have been increasingly employed in bridge engineering over the past few decades, mainly due to the following: (1) the capability of enhancing seismic performance through significant energy dissipation, (2) no change in the stiffness characteristics of the main structure, and (3) better suited to suppress structural response under near-fault ground motions.

However, when the actual displacement exceeds the stroke of the viscous damper, the pounding within the damper will generate pounding force that may lead to the failure of the viscous damper. For example, in the 2011 Great East Japan earthquake, the viscous dampers installed on the first floor of the administration building located on the campus of the Tohoku Institute of Technology in Japan were completely destroyed. This is the first report of viscous dampers failing in service due to the earthquakes [12, 13], as shown in Figure 1. The researchers concluded that earthquakes exceeding the considered level resulted in excessive pounding force generated by the insufficient stroke limit, leading to the damage of the dampers. Miyamoto et al. [14] conducted an experimental investigation to analyze the limit

states of the viscous dampers. When the actual displacement exceeds the limit stroke, the metal parts at the upper or lower half of the damper would lead to excessive pounding force on the cylinder wall and cause damage to the viscous damper.

In order to reduce the pounding force, the researchers filled the second chamber of the viscous damper with metallic springs or inert gases; [15] however, both methods have obvious drawbacks. For metallic springs, the stiffness coefficient is constant. Too high or too low stiffness cannot solve the problem and may affect the energy dissipation capacity of the viscous dampers. Thus, materials with variable stiffness are more suitable for use as bumpers than those with constant stiffness. For inert gases, despite their variable stiffness properties, this method necessitates very strict sealing, and once the sealing fails, it cannot achieve the desired effect. Rubber has been widely used in bridge engineering as a variable stiffness bumper, which does not necessitate strict sealing conditions [16, 17]. However, rubber has poor durability and its performance will deteriorate due to aging effects during its service life, and the heat generated by the viscous damper during working will further accelerate the aging of rubber [18]. Metal rubber [18–21] is a porous material composed of stainless-steel metal wire, possessing excellent elasticity and energy absorption capability. Compared to rubber, metal rubber is capable of adapting to corrosive, extreme high and low temperatures, and other hostile environments. Because of its outstanding performance, metal rubber has been widely utilized in military and aerospace fields. Recently, the vibration control devices in bridge engineering based on metal rubber have gained attention from scholars [18, 19]. Nonetheless, the effectiveness of metal rubber as a bumper to reduce the pounding force in dampers has not been extensively investigated.

Seismic performances of bridge engineering were usually evaluated by conventional seismic testing methods, i.e., quasistatic testing [22], pseudodynamic testing [23], and shaking table testing [24, 25]. Due to the slow loading rate, quasistatic testing and pseudodynamic testing cannot be performed on velocity-related dampers. Due to the limitations of the testing equipment, shaking table testing usually requires the specimen to be designed in small scale. Real-time hybrid testing (RTHT) separates a structural system into at least one numerical substructure (NS) and one experimental substructure (ES) [26, 27]. The part of the structure that can be precisely simulated is taken as NS, while the rest part of the structure is taken as ES. Thus, RTHT can be performed on a large-scale or even full-scale structural model. The response of the structure is obtained by real-time loading of the actuators and solving the equations of motion in the computation device. The pounding effect has a high-frequency characteristic, necessitating a relatively large sampling frequency for an accurate capture. However, the maximum sampling frequency of the loading equipment is usually only 2048 Hz. The resampling may cause stability issues in RTHT, such as the stability of integration algorithms, the accumulation of errors, and time delay compensation. As far as the authors know, no RTHT that take the pounding effect into account has been carried out thus far.

1.2. Scope. From the previous background introduction, it is evident that although inert gases and metallic springs have been employed to mitigate the pounding force, both methods have obvious drawbacks, thus necessitating the proposal of a novel viscous damper to address the aforementioned problems. Moreover, before conducting RTHT that take the pounding effect into consideration, it is necessary to perform real-time hybrid simulation (RTHS) that can more realistically reflect the test process to check the feasibility of the test and make predictions about the results.

In this paper, a novel viscous damper will be introduced in Section 2 and the working mechanism and load-displacement relationship of the novel damper will be explained in detail. Second, numerical simulations will be presented in Section 3 to investigate the seismic response of a bridge equipped with a novel viscous damper and compare with two different viscous dampers. Third, RTHS for considering the pounding effect of the novel viscous damper will be presented in Section 4. Finally, design recommendations will be proposed to provide references for pounding mitigation in Section 5.

2. Introduction of the Novel Viscous Damper Applied in Bridges

2.1. Construction of the Pounding Mitigation Mechanism in Dampers. As shown in Figure 2(a), a typical traditional viscous damper mainly consists of piston rod, piston head, cylinder, fluid, clevis, spherical bearings, and sealing rings. The functions of each part have been described in detail in the previous research [14]. Generally, it is advised that L_1 should be shorter than L_2 to prevent the piston rod from being pulled out of the second chamber. When the external displacement exceeds L_1, an additional axial pounding force is generated as a result of the pounding between the piston head and the cylinder.

The novel viscous damper mainly consists of two parts, i.e., the traditional viscous damper and the metal rubber bumpers, as shown in Figure 2(b). At the end of the piston rod, another piston head (marked as piston head 2) is provided to compress the metal rubber bumpers. The piston head 2 can be made of steel and its diameter should be slightly smaller than the inner diameter of the cylinder to ensure that the piston head can move flexibly in the axial direction. The strokes in the first and the second chamber are equal.

Multiple identical small metal rubber bumpers are arranged at both ends of the second chamber. Since the metal rubber bumpers are only subjected to compression, they can be bonded to the cylinder wall using a strong adhesive. The stiffness of metal rubber should not be too high or too low and should be easily adjusted. The constitutive model of the small metal rubber specimen can be obtained through compression testing; so, the expected

(a) (b)

Figure 1: Viscous damper destroyed in the 2011 Great East Japan earthquake (figure source: [12, 13]): (a) intact damper; (b) damaged damper.

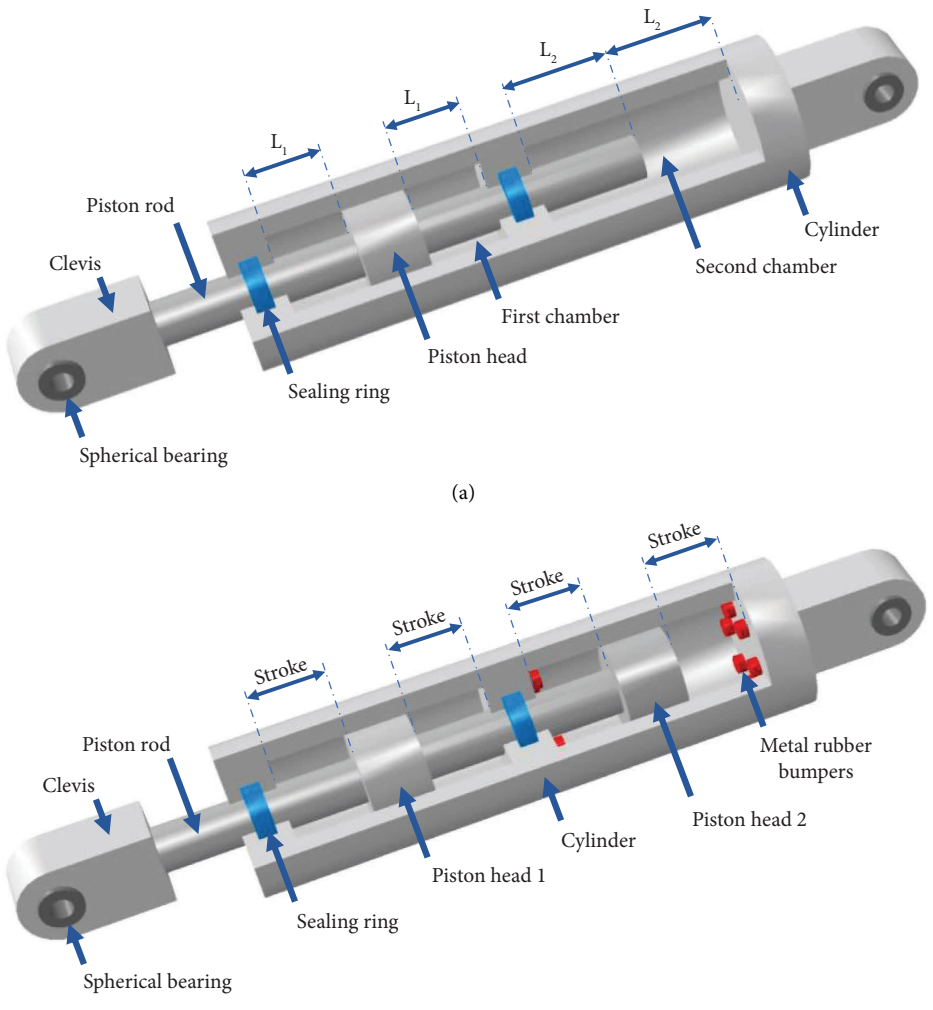

Figure 2: Traditional and novel viscous dampers: (a) traditional viscous damper and (b) novel viscous damper.

stiffness can be easily obtained by adjusting the number of small metal rubber bumpers. Its advantage is that it allows for greater flexibility in design. It is also feasible to replace multiple small metal rubber bumpers with a larger one, and the stiffness can be obtained by considering their geometric dimensions and the constitutive model. Furthermore, the metal rubber bumpers should be symmetrically arranged at both ends of the second chamber in order to make the force-displacement relationship of the novel viscous damper symmetrical in both tension and compression.

The first advantage of the novel viscous damper is that the load-displacement relationship of metal rubber has a distinct strain hardening characteristic, which does not affect the energy consumption of the viscous damper when

small deformation occurs but provides a large load for the viscous damper when large deformation occurs. Second, no strict sealing and complex manufacturing process is required, providing better performance at an acceptable cost. Third, the metal rubber can adapt to harsh environments such as corrosion, high and low temperatures, and has excellent durability. Metal rubber can meet the requirements of viscous dampers for long-term service and high temperature generation during working. Finally, metal rubber has excellent elasticity and energy dissipation ability, which can further dissipate energy in the pounding process.

2.2. Force-Displacement Relationships of Each Component

2.2.1. Viscous Damper Component. The typical relationship between damping force and velocity can be expressed as follows:

$$F_{ve} = C_{ve} \cdot (\dot{u})^{\alpha} \cdot \operatorname{sgn}(\dot{u}), \tag{1}$$

where F_{ve} is the force of the viscous element, C_{ve} is the damping coefficient, u is the axial displacement, and α is the damping exponent, which reflects the nonlinear degree of the damper. In most cases, the viscous damper with α in the range of 0.1–0.5 can be applied in bridge engineering to resist earthquakes [28, 29].

2.2.2. Metal Rubber. The mechanical properties of metal rubber are influenced by many factors, such as its manufacturing process and material properties. Several axial compression tests were conducted on a designed metal rubbers commercially supplied by Hebei Jinbo Electromechanical Technology Co., Ltd in China. Compression tests were conducted on an electronic universal testing machine with ±250 kN axial load capacity at the Analysis, Testing, and Computing Center of the Harbin Institute of Technology, as shown in Figure 3(a). The dimensions of the specimens are 17.2 mm × 17.2 mm × 17.2 mm, made of 06Cr19Ni10 stainless-steel wire with a wire diameter of 0.15 mm and a relative density (the ratio of the density of the metal rubber to the stainless-steel wire) of 0.45. Figures 3(b) and 3(c) show the photographs of the metal rubber specimen in this study.

As shown in Figure 4(a), the load-displacement curve of the metal rubber pads obtained from the tests exhibits an obvious strain hardening behavior. A simplified constitutive model based on the compression tests is shown in Figure 4(b), which has been employed in some previous studies [16, 17]. The cubic polynomial [30] was used to describe the loading curve. According to the geometric dimension of the specimens, the simplified model can be expressed as follows:

$$\begin{cases} \sigma_{\text{loading}} = 171.4\varepsilon_{mr}^3 + 357.2\varepsilon_{mr}^2 + 392.8\varepsilon_{mr}, \\ \sigma_{\text{unloading}} = \begin{cases} 9678.43\varepsilon_{mr}, & \sigma \neq 0, \\ 0, & \sigma = 0, \end{cases} \end{cases} \tag{2}$$

where σ_{mr} and ε_{mr} represent the stress and strain of the metal rubber, respectively.

A comparison of the stress-strain relationship between metal rubber and traditional rubber (from the reference [31]) is shown in Figure 5. Metal rubber has a higher elastic modulus, thereby preventing the premature failure of the bumper under rare earthquakes. It is noteworthy that the stress-strain relationship of the metal rubber is dependent on its density and can be adjusted to achieve the desired result.

2.2.3. Cylinder Wall. This component is used to model the limit state when the applied external displacement exceeds the specified damper stroke [14]. Generally, the cylinder wall can be considered as an elastic member with high stiffness, without considering the axial capacity and the lateral (hoop) stress. The mechanical properties of the cylinder wall can be expressed as follows:

$$F_{cw} = \begin{cases} K_{cw}(|u| - u_s)\operatorname{sgn}(u), & |u| \geq u_s, \\ 0, & |u| < u_s, \end{cases} \tag{3}$$

where F_{cw} is the axial force of the cylinder wall, K_{cw} is the stiffness of the cylinder wall, u is the axial displacement, and u_s is the available stroke.

2.3. Force-Displacement Relationships of the Novel Viscous Damper.

Since the novel viscous damper proposed in this study only focuses on reducing pounding force, it is assumed that the pounding force can be expressed as the output of the metal rubber, which can be obtained by multiplying the stress and cross-sectional area based on the constitutive model of the metal rubber bumper provided in equation (2). In other words, the piston rod is considered as a rigid body. Similar methods for calculating the pounding force have been used in previous references [15, 17, 19].

The mechanical model of the novel viscous damper is shown in Figure 6. C_{ve} represents the pure viscous element of the viscous damper. Gap_{mr} and Hook_{mr} represent the openings equal to the displacement from the neutral damper position to metal rubber. If the metal rubber dimensions of both ends are equal, then the initial values of Gap_{mr} and Hook_{mr} are opposite numbers. When the metal rubber undergoes plastic deformation, Gap_{mr} and Hook_{mr} will change. Hysteresis_{mr} is the hysteretic element of the metal rubber and K_{cw} is the stiffness of the cylinder wall.

Series force F_s and series displacement u_s of the metal rubber and the cylinder wall can be expressed as follows:

$$\begin{aligned} F_s &= F_{mr} = F_{cw}, \\ F_{mr} &= \sigma_{mr} A_{mr}, \\ F_{cw} &= K_{cw} u_{cw}, \\ u_s &= u_{mr} + u_{cw} = \begin{cases} u - \text{gap}_{mr}, & u > \text{gap}_{mr}, \\ u - \text{hook}_{mr}, & u < \text{hook}_{mr}, \end{cases} \end{aligned} \tag{4}$$

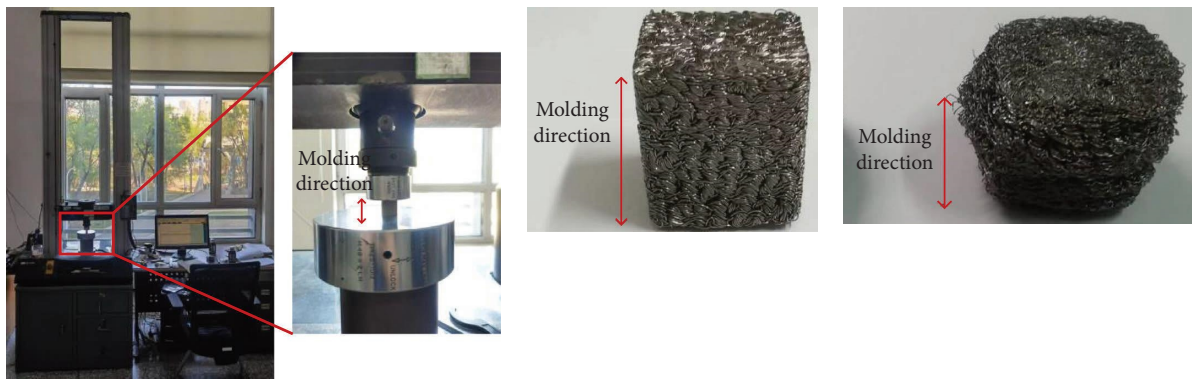

Figure 3: Metal rubber and test machine: (a) testing machine; (b) metal rubber specimen before testing; (c) metal rubber specimen after testing.

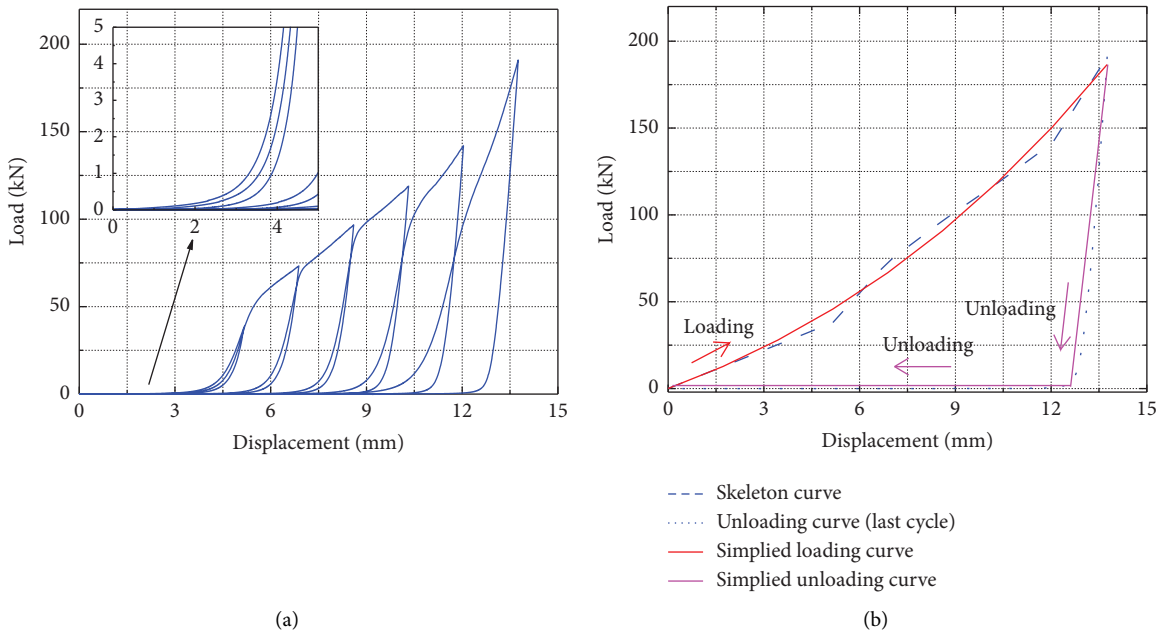

Figure 4: Experiment curve and simplified constitutive model: (a) experiment with metal rubber and (b) simplified constitutive model.

where F_{mr} is the force of the metal rubber, σ_{mr} is the stress of the metal rubber which can be calculated by equation (2), A_{mr} is the cross-sectional area of the metal rubber, u_{cw} is the displacement of the cylinder wall, and u_{mr} is the displacement of the metal rubber.

According to the discussion above, the force provided by the novel viscous damper can be expressed as follows:

$$F = \begin{cases} C_{ve} \cdot \operatorname{sgn}(\dot{u}) \cdot (\dot{u})^{\alpha} \left(\text{hook}_{mr} \le u \le \text{gap}_{mr}\right), \\ C_{ve} \cdot \operatorname{sgn}(\dot{u}) \cdot (\dot{u})^{\alpha} + F_s, \quad \text{else.} \end{cases} \tag{5}$$

3. Numerical Simulations

To illustrate the seismic performance of the novel viscous damper for bridges, this section investigates the response of a simply-supported girder bridge [32] with a span of 25 m equipped with the novel viscous damper subjected to earthquake. The superstructure is a prestressed reinforced concrete T-shape girder. Rectangular piers are used for the substructure. The length and width of the piers are 1 m × 0.75 m. Laminated rubber bearings connect the superstructure and the substructure. Without considering the deformation of the piers, the superstructure and bearings can be simplified to a single-degree-of-freedom system approximately. The fundamental frequency of the model is 0.876 Hz, which is consistent with the reference [32].

As shown in Figure 7, three models are established, respectively, with specific instructions as follows. Model I is equipped with the idealized viscous damper (the piston moves without stroke limit). Model II is equipped with the traditional viscous damper with the piston movement limit. Model III is equipped with the novel viscous damper proposed in this study. It is assumed that all viscous dampers are

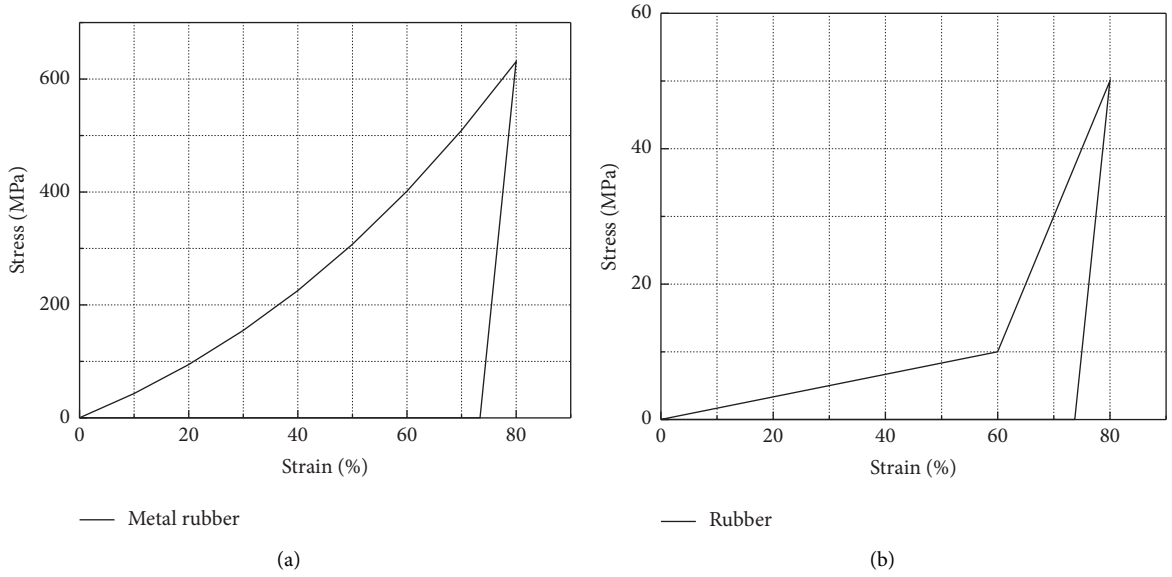

Figure 5: Comparison of stress-strain relationship: (a) metal rubber and (b) rubber.

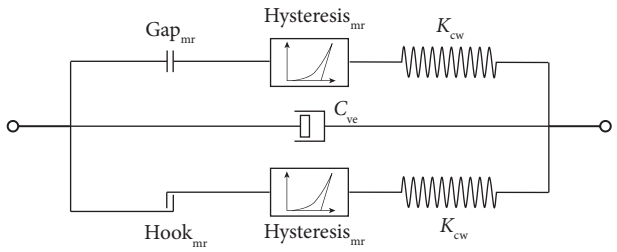

Figure 6: Mechanical model of the novel viscous damper.

not force limited and would not fail in an earthquake. The Kobe rarthquake wave is adopted as the input for ground motion and the peak ground acceleration has been adjusted to 620 gal. The comparison between the results from models I and II is made to investigate the effect of pounding on seismic responses, and the pounding mitigation effect of novel viscous damper is analyzed by comparing the results obtained from models II and III. The values and descriptions of the parameters are shown in Table 1.

3.1. Effect of Pounding on Seismic Responses. Figures 8(a)–8(c) show the displacement, velocity, and acceleration responses of model I and model II, respectively. The amplitudes of displacement, velocity, and acceleration responses of model I are 0.15 m, 0.86 m/s, and 8.01 m/s^2, respectively. The amplitudes of displacement, velocity, and acceleration responses of model II are 0.13 m, 0.81 m/s, and 10.60 m/s^2, respectively. The amplitude ratios of model I to model II are 1.15 : 1, 1.06 : 1, and 0.76 : 1, respectively. It is shown that the pounding effect did not significantly change the displacement and velocity response but significantly increased the acceleration response.

Figure 8(d) shows the fast Fourier transform (FFT) of the acceleration response. It is observed that the amplitude of Fourier power obviously increases in the frequency region from 0.6 Hz to 3.3 Hz when considering the pounding effect, indicating that the acceleration response between 0.6 Hz and 3.3 Hz is caused by the pounding of the traditional viscous damper. When the pounding occurs, the pounding members provide additional stiffness to the structure, which may contribute to the increased frequency response.

Figures 8(e) and 8(f) show the hysteresis curves of the viscous damper. The hysteresis curve of the idealized viscous damper is full, indicating its good energy dissipation capability. The maximum damping force is 327 kN however, the maximum distance of movement of the piston is 0.28 m, which is not economical. When the displacement of the traditional viscous damper reaches its stroke limit, pounding force is generated, which can reach a maximum of 2913 kN. Such excessive force can easily damage the viscous damper.

3.2. Pounding Mitigation Effect of Metal Rubber. The pounding amplifies the acceleration response of the structure and generates the pounding force, which may result in damage to the viscous dampers and even cause damage to the connectors. Metal rubber is selected as the bumper to mitigate the adverse effects of the pounding. It has strain hardening behavior and is more suitable for long-term use in viscous dampers due to its superior durability and stability when compared to rubber. Figure 9 shows a comparison of the responses of model II and model III. As shown in Figures 9(a) and 9(b), the displacement and velocity of the structure are decreased. This is mainly due to the decreased distance between the pounding members. Additionally, metal rubber bumpers also dissipate some energy during the pounding process.

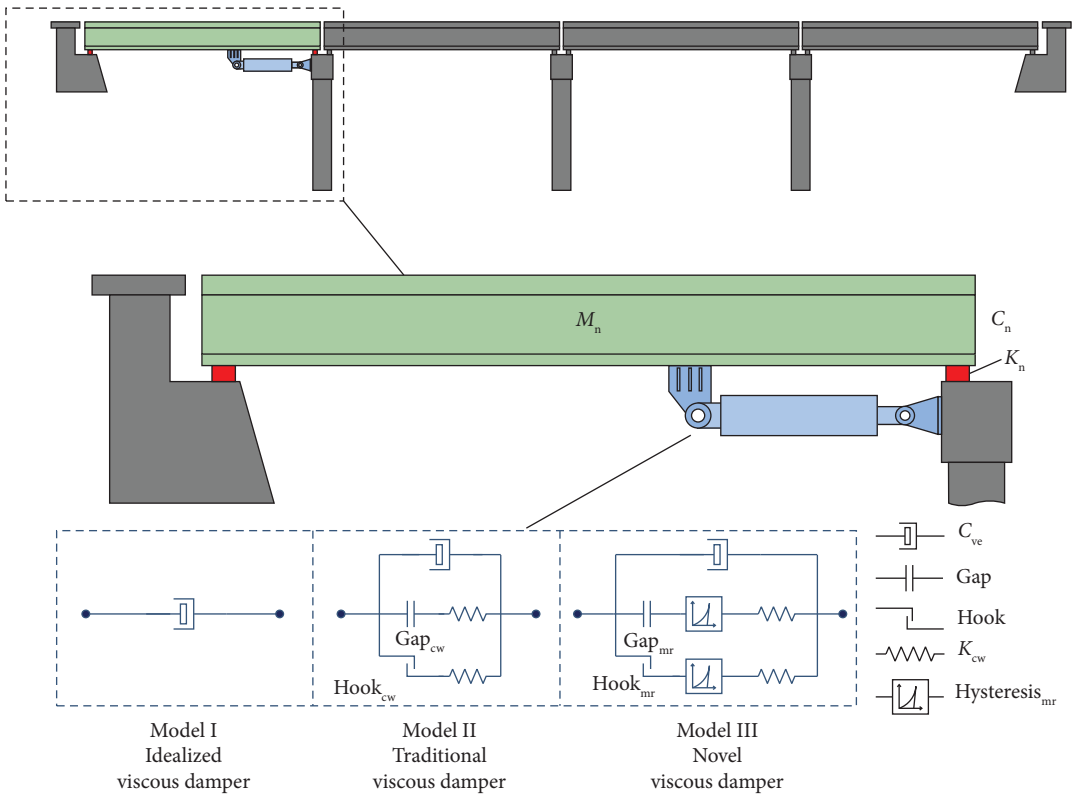

Figure 7: Schematic of the models.

Table 1: Main parameters of the model.

Parameters	Descriptions	Values
K_n	Stiffness of laminated rubber bearings	1.91×10^4 kN/m
C_n	Damping coefficient, calculated by the damping ratio of 5%	346 kN/(m/s)
M_n	Mass of superstructure	630 t
f	Fundamental frequency	0.876 Hz
C_{ve}	Pure viscous element of the viscous damper	354 kN/(m/s)$^{0.5}$
K_{cw}	Stiffness of the cylinder wall	1×10^5 kN/m
Gap$_{cw}$/Hook$_{cw}$	The available stroke	±0.1 m
Hysteresis$_{mr}$	Hysteretic element of metal rubber, which can be calculated according to equation (2) and the dimensions of metal rubber. The initial dimensions of the metal rubber are 12 cm × 12 cm × 6 cm	—
Gap$_{mr}$/Hook$_{mr}$	Equal to 0.6 times the available stroke	±0.06 m

As illustrated in Figure 9(c), after designing the metal rubber, the amplitude of acceleration is decreased from 10.6 m/s^2 to 7.98 m/s^2, a decrease of 25%. Figure 9(d) shows the FFT of the acceleration response. The Fourier power of acceleration in the majority of region from 0.6 Hz to 3.3 Hz is decreased after the installation of the metal rubber bumpers. Due to the stiffness of metal rubber bumpers typically being lower than that of the cylinder wall, when a pounding occurs, the metal rubber bumpers can significantly reduce the stiffness and natural frequency of the overall structure, as well as its frequency response. Figure 9(e) presents the time histories of the pounding force, indicating that the metal rubber bumpers significantly reduce the force from 2841 kN to 2159 kN, a decrease of 24%. However, the number of poundings increases because the distance between pounding members decreases. Figure 9(f) shows the hysteresis curve of the novel viscous damper. Before the pounding, the hysteresis curve is full, indicating the good energy dissipation capability of the novel viscous damper. The hysteresis curve has distinct buffer stages, and due to the residual deformation left by the metal rubber bumpers after elasto-plastic deformation, the initial positions of the buffer stages will change.

3.3. Parameter Analysis. The objective of bumpers is to mitigate undesirable effects caused by pounding force. Too high or too low stiffness of the bumper may fail to reduce the pounding force and may even result in an increase. To achieve this objective, it is essential to ensure that the stiffness of the metal rubber bumpers is within a reasonable range.

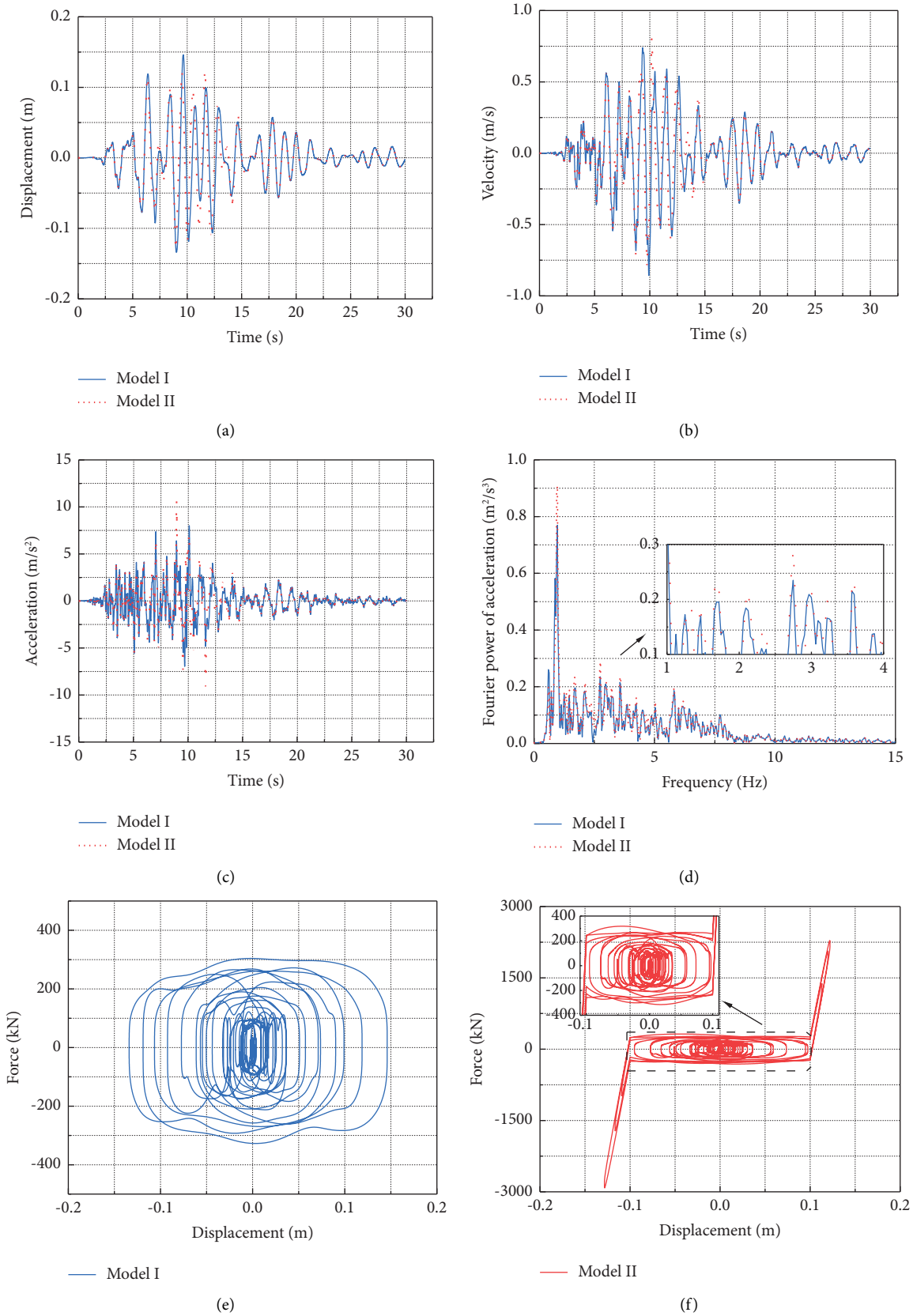

FIGURE 8: Comparisons between the results from models I and II: (a) displacement; (b) velocity; (c) acceleration; (d) FFT of acceleration; (e) hysteresis curve of the idealized damper; (f) hysteresis curve of the traditional damper.

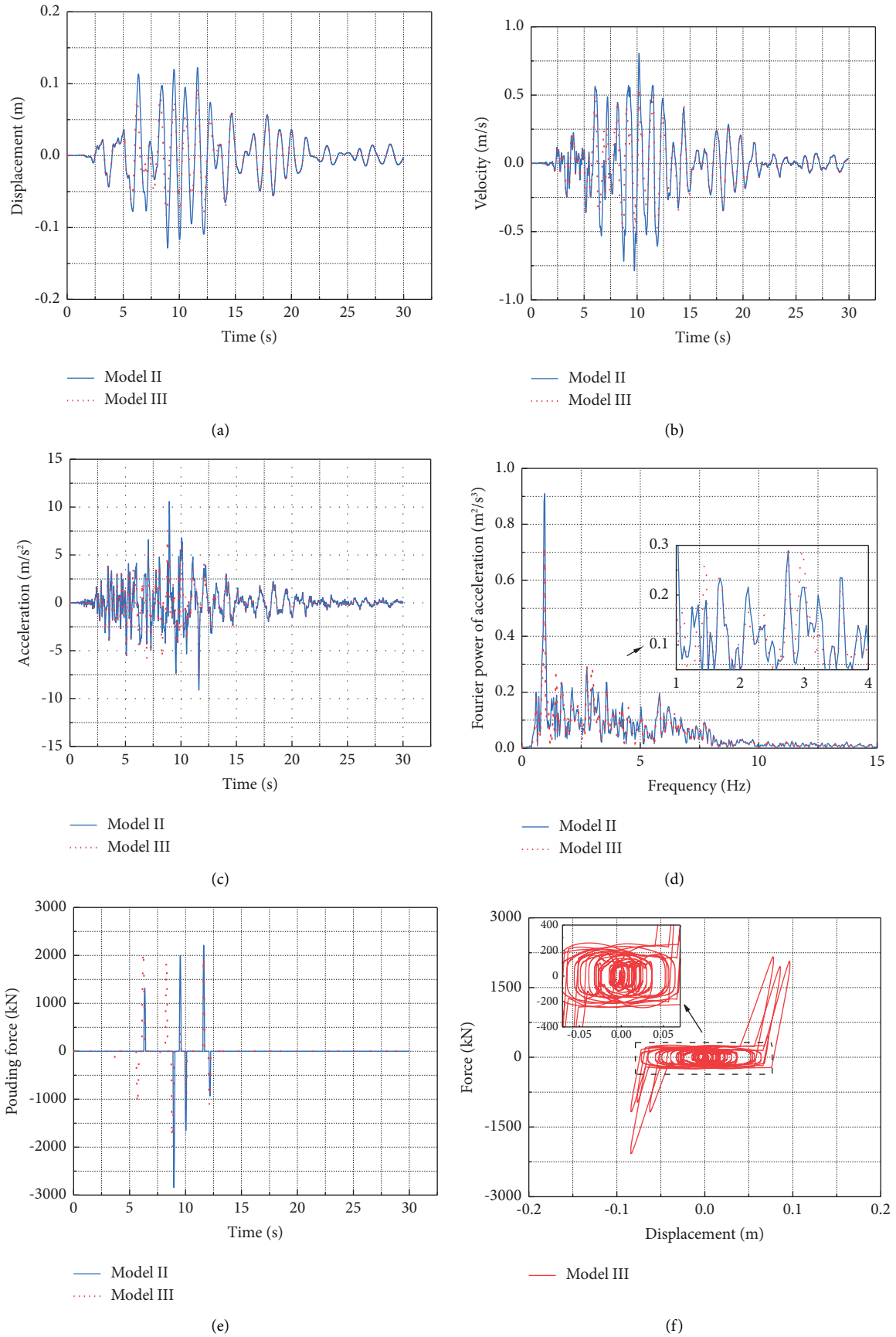

FIGURE 9: Comparisons between the results from models II and III: (a) displacement; (b) velocity; (c) acceleration; (d) FFT of the acceleration; (e) pounding force; (f) hysteresis curve of the new damper.

3.3.1. Influence of the Area of the Metal Rubber Bumpers. This subsection discusses the influence of the area of the metal rubber bumpers installed in the viscous damper. Six different cases are considered, with areas of 100, 125, 150, 175, 200, and 300 cm^2. Parametric studies are conducted on model III with a metal rubber thickness of 6 cm. The stress-strain model of metal rubber bumpers provided in equation (2) is used to derive the force-displacement relationship of bumpers with different areas.

The amplitudes of the pounding force with different metal rubber areas are shown in Figure 10(a). As the area decreases, the amplitude of the pounding force decreases gradually, which are directly caused by the lower stiffness of the metal rubber bumpers. However, the stiffness of the metal rubber bumpers should not be too low; otherwise, the metal rubber may fail under rare earthquake and cannot play the role in continuously mitigating the pounding. It should be noted that in all cases, the maximum strain of the metal rubber bumpers does not exceed 80%, as this strain is close to the failure of metal rubber in the experiments.

3.3.2. Influence of the Thickness of the Metal Rubber Bumpers. It is expected that increasing the thickness of metal rubber bumpers may help to reduce the pounding force but may result in more poundings and longer pounding duration. To identify the influence of the thickness of metal rubber bumpers on the pounding, five different metal rubber thicknesses are considered, which are 0.2, 0.35, 0.5, 0.65, and 0.8 times of the stroke. In these cases, the stroke is 10 cm and the area is 100 cm^2. The stress-strain model of metal rubber bumpers provided in equation (2) is used to derive the force-displacement relationship of bumpers with different thickness.

The amplitudes of the pounding force with different metal rubber thickness are given in Figure 10(b). As the thickness of the metal rubber increases, the pounding force decreases significantly. This is because increasing the thickness will decrease the stiffness of the metal rubber, which helps to reduce pounding force and high-frequency response of the structure. When the thickness of metal rubber bumpers is within 0.2–0.5 times of the stroke, the pounding force significantly decreases with the increase in thickness. However, when the metal rubber thickness exceeds 0.5 times of the stroke, the mitigation efficiency gradually decreases. Obviously, a greater thickness is not economical, which also reflects the need for the effective design of metal rubber bumpers to provide a reasonable pounding mitigation effect.

4. Real-Time Hybrid Simulation

In order to more precisely reveal the performance of the novel viscous damper, RTHT may be the best choice. The pounding effect has a high-frequency characteristic, necessitating a relatively large sampling frequency for accurate capture. However, the maximum sampling frequency of the loading equipment is usually only 2048 Hz. The resampling of the loading equipment may cause stability issues in RTHT, such as the stability of integration algorithms, the accumulation of errors, and time delay compensation. Hence, it is essential to conduct RTHS which can accurately reflect the testing process. This helps to minimize the adverse effects or even damage to the experimental system from unknown failure modes of the components or structures in the test.

4.1. Electrohydraulic Servo Loading System. The electrohydraulic servo loading system is a widely utilized loading equipment for seismic tests, which is a complex system containing nonlinear factors, such as electrohydraulic conversion, throttling characteristics of control elements, and amplitude limitation. The nonlinear characteristics performance of the electrohydraulic servo loading system will greatly affect the results of RTHT. Therefore, a model that can more realistically reflect the characteristics of the electrohydraulic servo loading system is established.

4.1.1. PID Controller. The loading of the ES is controlled by displacement, and the controller in the electrohydraulic servo loading system is the PID control. The displacement command is converted into an electrical signal by the controller, and the electrical signal from the controller is sent to the servo valve. The mathematical expression as the Laplace transform is as follows:

$$i_{\mathrm{PID}}(s) = \left(P + I\frac{1}{s} + Ds\right)e(s), \tag{6}$$

where $i_{\mathrm{PID}}(s)$ is the output control signal and $e(s)$ is the feedback error. The parameters P, I, and D are the proportional, derivative, and integral gains, respectively. In this paper, the parameters are set to 40, 0.025, and 0.1.

4.1.2. Servo-Valve and Hydraulic Actuator. The simplified layout of a servo-valve and hydraulic actuator is shown in Figure 11. The controller signal $i_{\mathrm{PID}}(s)$ provided by the controller caused the displacement of the spool. The orifice opening is determined by the spool displacement x_s, and it controls the direction and rate of the hydraulic fluid q_A and q_B. The oil pressures in both chambers, P_A and P_B, can be determined by solving equations related to the volume of the oil flow to the chamber pressure and the position of the piston rod. The piston force r_p is being applied to the ES.

The maximum force, displacement, and velocity of the actuator in this paper are 500 kN, 0.127 m, and 0.528 m/s, respectively. The system parameters shown in Table 2 are cited from reference [33].

4.2. Real-Time Hybrid Testing System. Structural division and the RTHT system of a single-degree-of-freedom bridge structure with a novel viscous damper are illustrated in Figure 12. Structural parameters are consistent with Table 1, and the model of novel viscous damper is consistent with model III of Figure 7. Since the pounding force is excessive and the maximum force capacity of the actuator is only ±500 kN, the original model must be scaled. The scale factors are presented in Table 3.

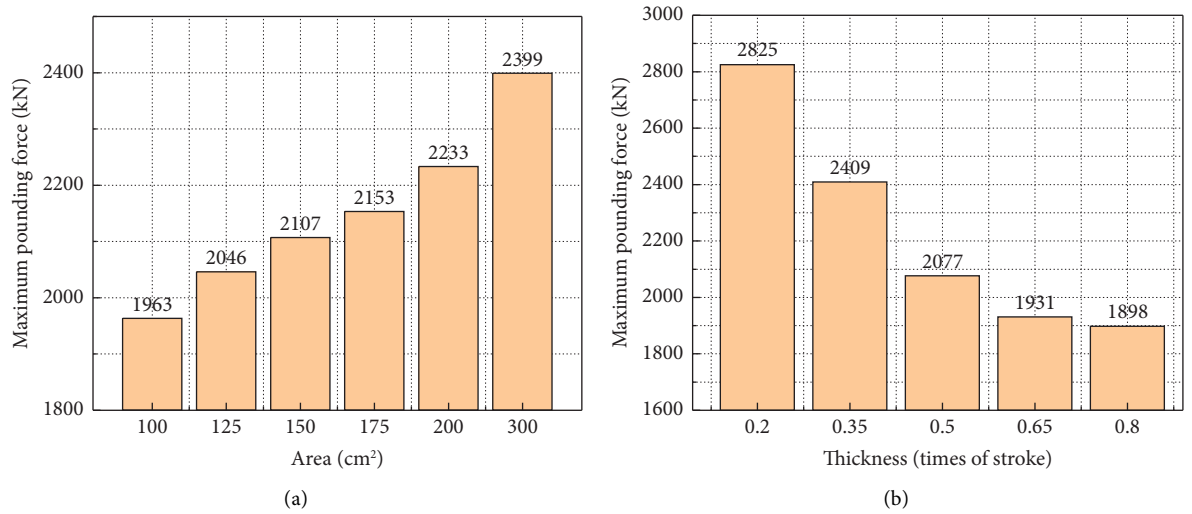

FIGURE 10: Comparison of the maximum pounding force: (a) area of the metal rubber bumpers and (b) thickness of the metal rubber bumpers.

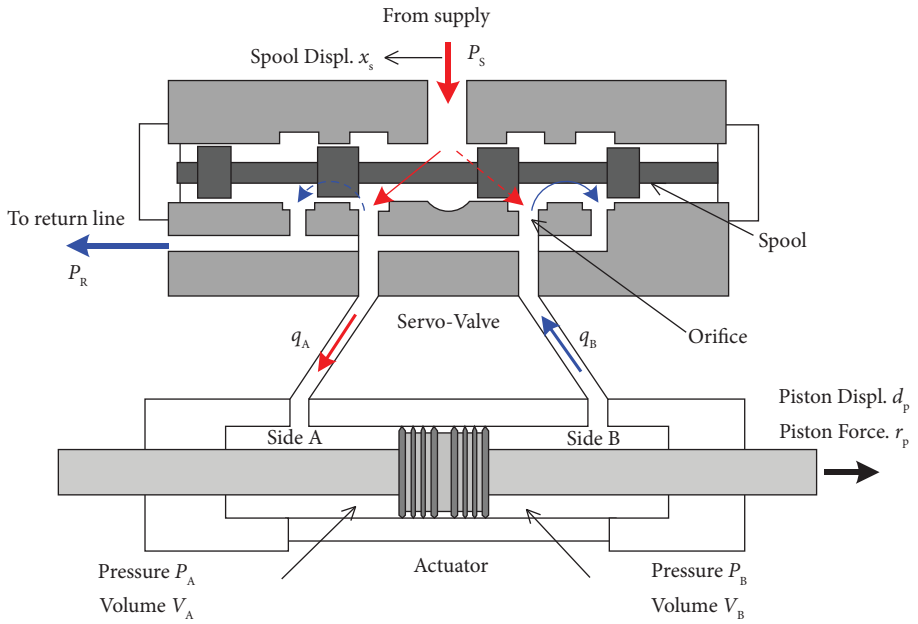

FIGURE 11: Simplified layout of a servo-valve and hydraulic actuator (figure source [33]).

TABLE 2: System parameters in simulations.

Parameters	Values
Servo-valve	
Damping ratio, ζ_S	70%
Natural frequency, ω_s (rad/s)	$130 \times 2\pi$
Discharge coefficient, k_v (in.^{4}/s·lb$^{0.5}$)	21.915
Supply pressure, P_S (psi)	3000
Return pressure, P_R (psi)	50
Actuator	
Piston area, A_P (in.^{2})	38.48
Length, l (in.)	10
Effect bulk modulus, β (psi)	100000

The modified central difference method [34] is employed as the integration algorithm, which is an explicit method that can avoid iterative solution. The time step is a set of 1/1024 s. Gaussian white noise with a mean square error of 0.5% of the standard deviation of the measured signal is added to the force transducer on the actuator to simulate the real test environment.

4.3. Results. Figures 13(a) and 13(b) show the comparison of displacement and velocity of the damper between RTHS and reference results. The reference results are obtained by adjusting the results of pure numerical simulation based on

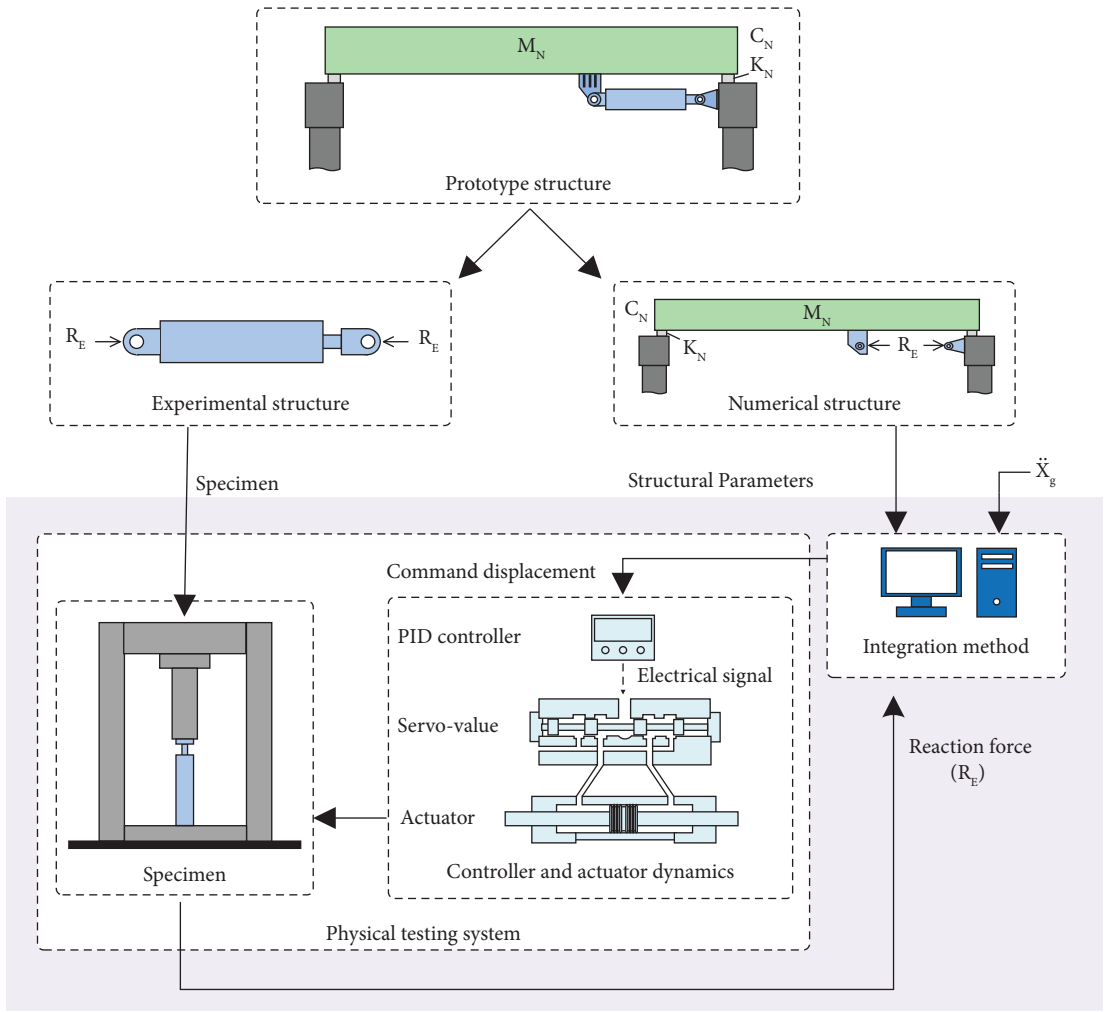

Figure 12: Real-time hybrid testing system of the novel viscous damper.

the scale factors. Figure 13(c) compares the acceleration of the structure between RTHS and reference results. To evaluate the accuracy of RTHS, AMP, RMSD, and K_{xy} are used to analyze the simulation results. The relevant equations are expressed as follows:

$$\text{AMP} = \frac{\max|x(i) - y(i)|}{\max|y(i)|} \times 100\%,$$

$$\text{RMSD} = \frac{\sqrt{\sum_{i=1}^{N}[x(i) - y(i)]^2}}{\sqrt{\sum_{i=1}^{N}[y(i)]^2}} \times 100\%, \tag{7}$$

$$K_{xy} = \frac{\sum_{i=1}^{N} x(i) \times y(i)}{\sqrt{\sum_{i=1}^{N} x^2(i) \times \sum_{i=1}^{N} y^2(i)}} \times 100\%,$$

where x is the comparison object, y is the reference object, i is the number of integration step, N is the total number of integration steps, AMP is the normalized error peak value which reflects the local error; RMSD is the normalized root-mean-square deviation which reflects the global error, and K_{xy} represents the correlation coefficient which reflects the degree of coincidence between the two curves. The calculation results are shown in Table 4.

Table 3: Scale factors.

Physical quantities	Scale factors
Modulus of elasticity	1
Length	0.1428
Density	4
Concentrated force	0.0204
Acceleration	1.75
Time	0.2857
Mass	0.0117
Stiffness	0.1429
Velocity	0.5

It can be seen from Table 4 that the K_{xy} of displacement and acceleration are both greater than 99%, and the AMP and RMSD are less than 6%. Although the pounding generated acceleration peaks, the RTHT system is able to track the acceleration and frequency response well, as shown in Figures 13(c) and 13(d). Good agreement can be seen in the hysteretic curve of the metal rubber shown in Figure 13(f), indicating that the RTHT system developed in this paper can

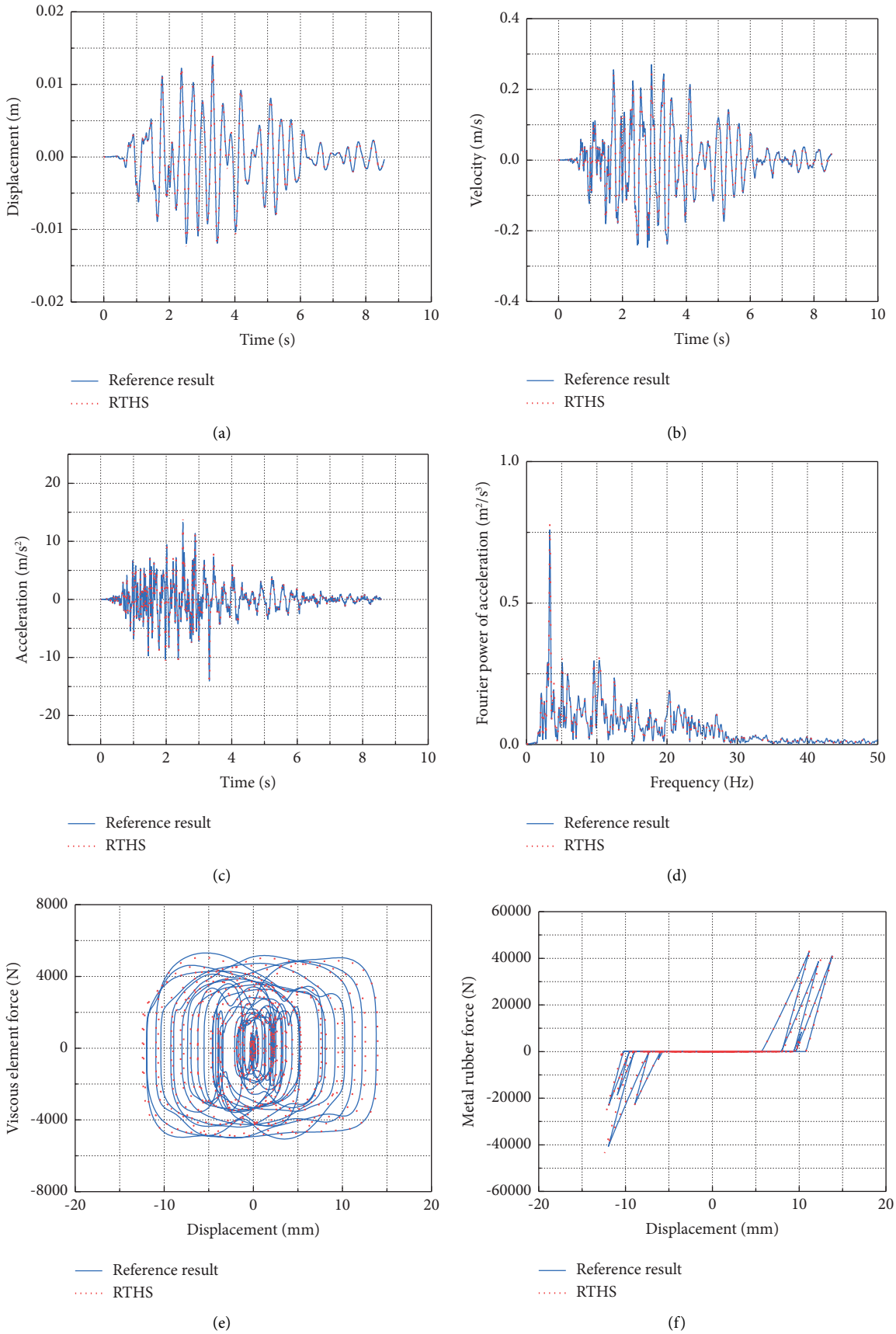

FIGURE 13: Comparison between RTHS and reference results: (a) displacement; (b) velocity; (c) acceleration; (d) FFT of the acceleration; (e) hysteresis curve of the pure viscous element; (f) hysteresis curve of the metal rubber.

Table 4: Error analysis.

Parameters	AMP (%)	RMSD (%)	K_{xy} (%)
Displacement	1.08	5.17	99.88
Velocity	10.18	6.94	99.85
Acceleration	1.32	5.51	99.86

effectively simulate the metal rubber bumpers with strong nonlinearity.

It should be noted that the velocity between RTHS and reference results matches well globally, as shown in Figure 13(b); however, the local error is relatively large. The AMP of velocity between RTHS and reference results is as high as 10.18%. The same issue is evident in the hysteresis curve of the pure viscous element in Figure 13(e). Reducing the time step can effectively decrease the global and local errors in velocity. However, the time step cannot be too small; otherwise, it will not meet the maximum sampling frequency of the hardware in actual testing. RTHS cannot match the response of the velocity very well, indicating that the proposed damper considering the pounding effect imposes new requirements to the RTHT method.

5. Design Recommendations for Pounding Mitigation

Based on the abovementioned analysis, metal rubber bumpers can effectively reduce the pounding force and high-frequency response of the structure. Two design recommendations are suggested to provide reference for pounding mitigation.

(1) Under the rare earthquakes not exceeding the design level, metal rubber should remain in the elastic stage as far as possible. The goal of the pounding mitigation design is to deal with rare earthquakes exceeding the design level. The mitigation effect will be decreased if the bumpers enter the plastic too early. According to the previous research, the maximum elastic strain of the metal rubber is approximately within 30%–40%, so 30% can be used a reasonable critical value for design.

(2) Metal rubber bumpers should not fail under rare earthquakes that exceed the design level. According to the experiment results, when the strain reaches 80%, the metal rubber is close to the failing. It is suggested that the ultimate strain of metal rubber should not exceed 80%.

6. Conclusion

In this paper, a novel viscous damper is proposed to address the issue of excessive pounding force generated when displacement exceeds the stroke limit. Based on a simplified bridge model, the advantages of the novel damper during an earthquake are demonstrated. The influence of geometric parameters of metal rubber on the pounding mitigation is discussed. RTHS is conducted to provide a basis for subsequent actual tests. Finally, the design recommendations for metal rubber bumpers are given. The main conclusions are as follows:

(1) The novel viscous damper proposed in this paper can effectively mitigate the pounding and protect the viscous damper from being damaged due to excessive pounding force. Through theoretical analysis and experimental studies, the force-displacement relationship of the novel damper is derived.

(2) In the numerical simulation of a simply-supported girder bridge, the pounding generates large force, which may cause damage to the traditional viscous damper. The novel viscous damper effectively reduced the amplitudes of pounding force and acceleration by 25% and 24%, respectively. The Fourier power of acceleration decreases in the region from 0.6 Hz to 3.3 Hz. The area and thickness of metal rubber bumpers need to be effectively designed to provide reasonable stiffness, which is beneficial in mitigating pounding.

(3) The results of RTHS show that the RTHT system developed in this paper can well simulate the pounding effect, and the RMSD of displacement, velocity, and acceleration between RTHS and reference results are all less than 7%. However, the AMP of the velocity between RTHS and reference results exceeds 10%, indicating that the proposed damper considering the pounding effect imposes new requirements to the RTHT method.

(4) Two design recommendations are proposed as references for the pounding mitigation design of the novel viscous damper.

Data Availability

The data used to support the findings of this study are available on request from the corresponding author.

Conflicts of Interest

The authors declare that they have no conflicts of interest.

Acknowledgments

The authors gratefully acknowledge the financial support provided by the National Natural Science Foundation of China (Grant no. 51978213) and the National Key Research and Development Program of China (Grant nos. 2017YFC0703605, 2016YFC0701106).

References

[1] L. Zu, Y. Huang, W. Li, H. Zhang, and L. Cai, "Seismic damage analysis of Yematan Bridge under near-fault earthquakes," *Structures*, vol. 41, pp. 586–601, 2022.

[2] W. Wang, Z. Yang, X. Hua, Z. Chen, X. Wang, and G. Song, "Evaluation of a pendulum pounding tuned mass damper for seismic control of structures," *Engineering Structures*, vol. 228, Article ID 111554, 2021.

[3] C. Yang, Z. Chen, W. Wang, X. Hua, and Y. Wang, "Optimal design of two viscous dampers for multi-mode control of a cable covering broad frequency range," *Engineering Structures*, vol. 245, Article ID 112830, 2021.

[4] N. Xiang, Y. Goto, M. Obata, and M. S. Alam, "Passive seismic unseating prevention strategies implemented in highway bridges: a state-of-the-art review," *Engineering Structures*, vol. 194, pp. 77–93, 2019.

[5] Y. Xu, C. Tong, and J. Li, "Simplified calculation method for supplemental viscous dampers of cable-stayed bridges under near-fault ground motions," *Journal of Earthquake Engineering*, vol. 25, no. 1, pp. 65–81, 2021.

[6] S. Mahjoubi and S. Maleki, "Pipe dampers as passive devices for seismic control of isolated bridges," *Structural Control and Health Monitoring*, vol. 24, no. 2, Article ID e1869, 2017.

[7] X. Shi, X. Guan, W. Shen, and L. Xing, "A control strategy using negative stiffness and semi-active viscous damping for fully tracking active control force for bridge cables: principles and simulations," *Structural Control and Health Monitoring*, vol. 29, no. 9, Article ID e2989, 2022.

[8] L. Chen, F. Di, Y. Xu, L. Sun, Y. Xu, and L. Wang, "Multimode cable vibration control using a viscous-shear damper: case studies on the Sutong Bridge," *Structural Control and Health Monitoring*, vol. 27, no. 6, Article ID e2536, 2020.

[9] I. Takewaki and H. Akehashi, "Comprehensive review of optimal and smart design of nonlinear building structures with and without passive dampers subjected to earthquake loading," *FRONT BUILT ENVIRON*, vol. 7, 2021.

[10] H. Akehashi and I. Takewaki, "Bounding of earthquake response via critical double impulse for efficient optimal design of viscous dampers for elastic-plastic moment frames," *JPN ARCHIT REV*, vol. 5, no. 2, pp. 131–149, 2022.

[11] H. Akehashi and I. Takewaki, "Resilience evaluation of elastic-plastic high-rise buildings under resonant long-duration ground motion," *JPN ARCHIT REV*, vol. 5, no. 4, pp. 373–385, 2022.

[12] L. Xie, M. Cao, N. Funaki, H. Tang, and S. Xue, "Performance study of an eight-story steel building equipped with oil dampers damaged during the 2011 great east Japan earthquake part 1: structural identification and damage reasoning," *Journal of Asian Architecture and Building Engineering*, vol. 14, no. 1, pp. 181–188, 2015.

[13] M. Cao, H. Tang, N. Funaki, and S. Xue, "Study on a real 8F steel building with oil damper damaged during the 2011 Great East Japan Earthquake," in *Proceedings of the World Conference on Earthquake Engineering*, 2012.

[14] H. K. Miyamoto, A. S. J. Gilani, A. Wada, and C. Ariyaratana, "Limit states and failure mechanisms of viscous dampers and the implications for large earthquakes," *Earthquake Engineering & Structural Dynamics*, vol. 39, no. 11, pp. 1279–1297, 2010.

[15] H. Zhang and X. Liu, "Investigation of the seismic behaviours of three-dimensional high-rise steel frame structures equipped with oil dampers with variable stiffness," *Journal of Constructional Steel Research*, vol. 179, Article ID 106542, 2021.

[16] B. Shrestha, H. Hao, and K. Bi, "Effectiveness of using rubber bumper and restrainer on mitigating pounding and unseating damage of bridge structures subjected to spatially varying ground motions," *Engineering Structures*, vol. 79, pp. 195–210, 2014.

[17] M. Yang, D. Meng, Q. Gao, Y. Zhu, and S. Hu, "Experimental study on transverse pounding reduction of a high-speed railway simply-supported girder bridge using rubber bumpers subjected to earthquake excitations," *Engineering Structures*, vol. 196, Article ID 109290, 2019.

[18] X. Xia, S. Wu, S. Sun, Q. Du, and F. Long, "Lateral hysteretic behavior of a novel metal rubber bridge bearing," *Engineering Structures*, vol. 256, Article ID 114051, 2022.

[19] S. Li, A. Guo, H. Li, and C. Mao, "An analysis of pounding mitigation and stress waves in highway bridges with shape memory alloy pseudo-rubber shock-absorbing devices," *Structural Control and Health Monitoring*, vol. 23, no. 10, pp. 1237–1255, 2016.

[20] D. Zhang, F. Scarpa, Y. Ma, J. Hong, and Y. Mahadik, "Dynamic mechanical behavior of nickel-based superalloy metal rubber," *Materials & Design*, vol. 56, pp. 69–77, 2014.

[21] Q. Tan and G. He, "Stretching behaviors of entangled materials with spiral wire structure," *Materials and Design*, vol. 46, pp. 61–65, 2013.

[22] R. T. Leon and G. G. Deierlein, "Considerations for the use of quasi-static testing," *Earthquake Spectra*, vol. 12, no. 1, pp. 87–109, 1996.

[23] M. Hakuno, M. Shidawara, and T. Hara, "Dynamic destructive test of a cantilever beam, controlled by an analog-computer," *Proceedings of the Japan Society for Comparative Endocrinology*, vol. 1969, no. 171, pp. 1–9, 1969.

[24] A. Ceccotti, C. Sandhaas, M. Okabe, M. Yasumura, C. Minowa, and N. Kawai, "SOFIE project - 3D shaking table test on a seven-storey full-scale cross-laminated timber building," *Earthquake Engineering & Structural Dynamics*, vol. 42, no. 13, pp. 2003–2021, 2013.

[25] C. Qiu and S. Zhu, "Shake table test and numerical study of self-centering steel frame with SMA braces," *Earthquake Engineering & Structural Dynamics*, vol. 46, no. 1, pp. 117–137, 2017.

[26] M. Nakashima, H. Kato, and E. Takaoka, "Development of real-time pseudo dynamic testing," *Earthquake Engineering & Structural Dynamics*, vol. 21, no. 1, pp. 79–92, 1992.

[27] B. Wu, Z. Wang, and O. S. Bursi, "Actuator dynamics compensation based on upper bound delay for real-time hybrid simulation," *Earthquake Engineering & Structural Dynamics*, vol. 42, no. 12, pp. 1749–1765, 2013.

[28] Z. Lu, Z. Wang, Y. Zhou, and X. Lu, "Nonlinear dissipative devices in structural vibration control: a review," *Journal of Sound and Vibration*, vol. 423, pp. 18–49, 2018.

[29] D. De Domenico, G. Ricciardi, and I. Takewaki, "Design strategies of viscous dampers for seismic protection of building structures: a review," *Soil Dynamics and Earthquake Engineering*, vol. 118, pp. 144–165, 2019.

[30] Y. Li, X. Huang, and M. Wenxiong, "A theoretical model and experimental investigation of a nonlinear constitutive equation for elastic porous metal rubbers," *Mechanics of Composite Materials*, vol. 41, no. 4, pp. 303–312, 2005.

[31] K. Kawashima and G. Shoji, "Effect of restrainers to mitigate pounding between adjacent decks subjected to a strong ground motion," in *Proceedings of the 12th World conference*

on earthquake engineering-12WCEE, Auckland, New Zealand, Januray 2000.

[32] B. Song, Y. Ma, Z. Zhang, and R. Wang, "Study on the impact characters of beam and abutment and the measures against collision and falling beam under strong earthquake," *China Civil Engineering Journal*, pp. 5168–5175, 2018.

[33] R. Jung, *Development of Real-Time Hybrid Test System*, University of Colorado Department of Civil, Environmental, and Architecture Engineering, Colorado, 2005.

[34] B. Wu, H. Bao, J. Ou, and S. Tian, "Stability and accuracy analysis of the central difference method for real-time substructure testing," *Earthquake Engineering & Structural Dynamics*, vol. 34, no. 7, pp. 705–718, 2005.